PCCP

PAPER

Cite this: *Phys. Chem. Chem. Phys.*, 2016, **18**, 26291

Effect of a triplet to singlet state interaction on photofragmentation dynamics: highly excited states of HBr probed by VMI and REMPI as a case study†

Pavle Glodic,[a] Dimitris Zaouris,‡[a] Peter C. Samartzis,[a] Arnar Hafliðason[b] and Ágúst Kvaran*[b]

Received 13th June 2016,
Accepted 22nd August 2016

DOI: 10.1039/c6cp04108f

www.rsc.org/pccp

Analysis of mass resolved spectra as well as velocity map images derived from resonance enhanced multiphoton ionization (REMPI) of HBr *via* resonance excitations to mixed Rydberg ($6p\pi\ ^3\Sigma^-(v'=0)$) and valence (ion-pair) ($V\ ^1\Sigma^+(v'=m+17)$) states allows characterization of the effect of a triplet-to-singlet state interaction on further photoexcitation and photoionization processes. The analysis makes use of rotational spectra line shifts, line intensity alterations, kinetic energy release spectra as well as angular distributions. Energy-level-dependent state mixing of the resonance excited states is quantified and photoexcitation processes, leading to H^+ formation, are characterized in terms of the states and fragmentation processes involved, depending on the state mixing.

I. Introduction

While molecular photodissociation studies have mostly been associated with excitations to relatively low energy states, there is a growing interest in the effects of higher energy Rydberg states in this context. Due to an increasing density of states, state mixing is gradually playing a more important part in photofragmentation processes as excitation energy increases. This can involve interactions between Rydberg and valence states or between different Rydberg states. The effect of such high energy state interactions on further photodissociation, as well as photoionization processes, is largely an unexplored but very interesting research area.

UV/Vis spectra of hydrogen halides are rich in structured, vibrationally and rotationally resolved electronic spectra due to transitions to Rydberg as well as ion-pair valence states.[1–24] The frequently observed perturbation effects, appearing as line-shifts, line intensity and/or linewidth alterations, are indicative of state interactions and photodissociation processes. Thus, the hydrogen halides have turned out to be ideal candidates for studying state interactions and their effects on photodissociation and photoionization processes, involving molecular Rydberg states on a quantum state level basis.[2,3,5,8,9,12,16,19–31] A similar work on superexcited states of O_2 has been reported by Ehresman *et al.*[32,33] and Mo *et al.*[34]

Mass resolved REMPI spectra of hydrogen halides reveal a number of interactions between Rydberg states and ion-pair valence states of varying strength and nature.[2,3,5,8,9,13,14,16–25,35,36] Evidence of Rydberg–Rydberg state interactions has also been reported.[29] Direct predissociation of the Rydberg states through repulsive valence states is found to be common as well as indirect predissociation, *via* state interactions, of ion-pair states and Rydberg states. State interactions have been interpreted in terms of level-to-level interactions between quantum states of the same total angular momentum quantum numbers, J'.[18,22–24,29,30] Weak interactions are normally limited to near-degenerate levels, which, typically, appear as line-shifts or line-intensity alterations for one to three rotational lines only, in line series. The effects of stronger interactions on the other hand, can be seen for non-degenerate levels, hence a range of spectral lines. "Non-degenerate interactions", typically, are found for states of equal symmetries ($\Delta\Omega = \Delta\Lambda = \Delta\Sigma = 0$), whereas "near-degenerate interactions" can be found for different state symmetries. The interaction between the $6p\pi\ ^3\Sigma^-(0^+; v'=0)$ Rydberg state and the $V^1\Sigma^+(0^+; v'=m+17)$ ion-pair state for HBr is an example of a "near-degenerate interaction" appearing as a slight shift of the Q rotational lines of the Rydberg state for $J'=7$ and 8 and as relative enhancement of the Br^+ ion signals compared to that of the HBr^+ signals for $J' \approx 8$.[21,37,38] The observed perturbation effects were used to identify and characterise the $V^1\Sigma^+(0^+; v'=m+17)$ state.[21]

[a] *Institute of Electronic Structure and Laser, Foundation for Research and Technology-Hellas, Vassilika Vouton, 71110 Heraklion, Greece*
[b] *Science Institute, University of Iceland, Dunhagi 3, 107 Reykjavík, Iceland. E-mail: agust@hi.is; Web: www.hi.is/~agust; Tel: +354-525-4800, +354-484-1259*
† Electronic supplementary information (ESI) available. See DOI: 10.1039/c6cp04108f
‡ Present address: Department of Physics and Astronomy, University College London, Gowen Street London WC1E, 6BT, UK.

Velocity map imaging (VMI) measurements, coupled with REMPI, of hydrogen halides have further revealed the effect of state interaction on photofragmentation of the mixed states. Thus, enhanced H^+ signals were observed in images of HCl recorded for the resonance excitations to two Rydberg states by changing the excitations from non-degenerate to near-degenerate energy levels.[27] Photofragmentation processes originating from the $E^1\Sigma^+(0^+; v' = 0)$ Rydberg and $V^1\Sigma^+(0^+; v')$ ion-pair states of HBr, and leading to $H^*(n = 2)$ and H^+ formation, have been found to depend on the "degree of energy level degeneracy".[30]

Based on the work by Loock *et al.*[39] and Zaouris *et al.*[30] the major paths for H^+ and HBr^+ formation by multiphoton excitation of HBr, following two-photon resonance excitations to Rydberg or ion-pair states (HBr**), involve one-photon excitation to superexcited Rydberg state(s) ($HBr^{\#}$) followed by:

$$HBr^{\#} \rightarrow H^*(n = 2) + Br^*/Br; \text{ dissociation}$$

$$H^*(n = 2) + h\nu \rightarrow H^+ + e^-; \text{ photoionization}$$

$$\text{channels } H^* + Br^*/Br \qquad (1a/1b)$$

$$HBr^{\#} \rightarrow HBr^{+*}(v^+)/HBr^+(v^+); \text{ autoionization}$$

$$HBr^{+*}(v^+)/HBr^+(v^+) + h\nu \rightarrow HBr^{+\#} \rightarrow H^+ + Br^*/Br; \text{ photodissociation}$$

$$\text{channels } HBr^{+*}/HBr^+. \qquad (2a/2b)$$

The kinetic energies released in the dissociation products H^* (1(a) and (b)) and H^+ (2(a) and (b)) typically vary as 1(a) < 1(b) < 2(a) ≈ 2(b) (see Fig. 1a). Br^+ formation is likely to involve the dissociation of a superexcited state to form Rydberg bromine atoms (Br**) followed by a one-photon photoionization, *i.e.*,

$$HBr^{\#} \rightarrow H + Br^{**}; \text{ dissociation}$$

$$Br^{**} + h\nu \rightarrow Br^+ + e^-; \text{ photoionization.} \qquad (3)$$

The relative contributions of various channels will depend on the nature of the resonance excited state HBr**. Typically, channels which give fragment ions *via* the neutral dissociative channels (1 and 3) are favoured in long range – hence ion-pair state – excitations, whereas both short and long range – hence both ion-pair and Rydberg states – excitations are likely to form the molecular ions. In the case of the strongly interacting $E^1\Sigma^+(0^+; v' = 0)$ and $V^1\Sigma^+(0^+; v')$ states[30] the relative contribution of the two dissociative H^+ formation channels (1(a) and 1(b)) is found to differ such that 1(a) is typically favoured for long-range – ion-pair state – excitations, whereas 1(b) is favoured for short-range – Rydberg state – excitations. This has been ascribed to varying contributions of different transitions to superexcited Rydberg states, which correlate with H^* + Br*/Br (Fig. 1b).[30] Furthermore, HBr^+ and HBr^{+*} are believed to be formed *via* autoionization of those Rydberg states, in which case low v^+ states of HBr^+ and HBr^{+*} are favoured for short-range (Rydberg state) excitations and higher v^+ are favoured for long-range (ion-pair) excitations. The energetics and relevant transitions are shown in Fig. 1b.

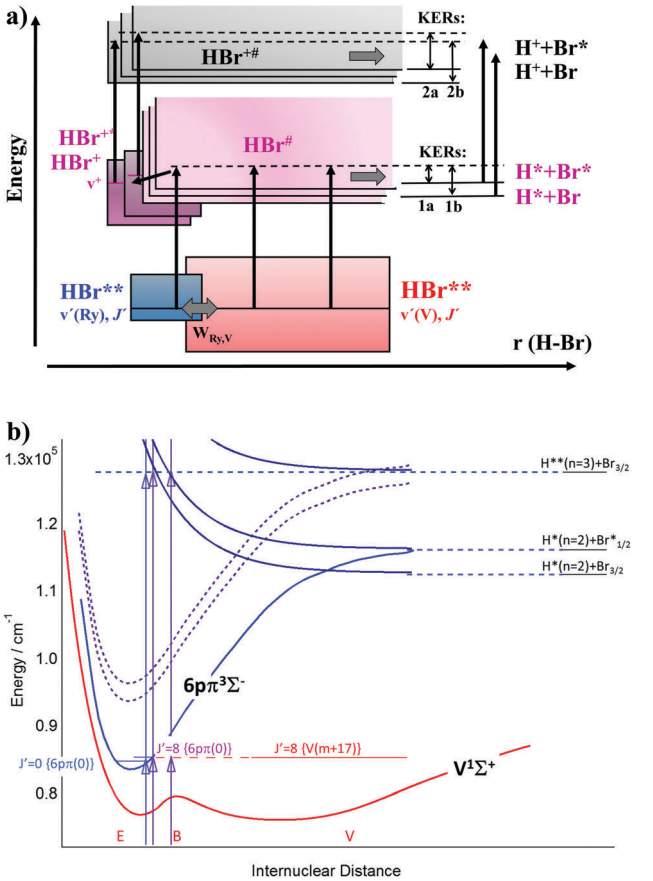

Fig. 1 (a) Schematic representation of the major H^+ formation channels based on VMI studies of (2 + *n*) REMPI of HBr following two-photon resonance excitations to the $E^1\Sigma^+$ Rydberg and $V^1\Sigma^+$ valence/ion-pair states (HBr**)[21–23,26,30] (see the main text for details). (b) Potential curves of the states involved in H^+ formations following two-photon resonance excitation of HBr to the 6pπ(0) and 6pπ(0)/V(*m* + 17) mixed state(s), asymptotic energies of fragments and relevant transitions (see the main text). The potential curve for the B states (red solid curve) was derived from Fig. 1 in ref. 39. The potential curves for the ionic states (broken curves) were derived from ref. 51. The shape of the ground ionic state was assumed to hold for the 6pπ Rydberg state (blue curve), whereas the shape of the repulsive states correlating with H* + Br/Br* and H** + Br are based on preliminary *ab initio* calculations,[54] which suggest that the curves might be of shapes close to that of the $B^2\Sigma$ ionic state.[51]

The focus of this paper is on revealing the connection between excited state interactions and further photodissociation and photoionization processes for interacting states with different spin quantum numbers. We use the 6pπ $^3\Sigma^-(0^+; v' = 0)$ Rydberg and $V^1\Sigma^+(0^+; v' = m + 17)$ ion-pair states for HBr (herein named as the 6pπ(0) and V(*m* + 17) states), mentioned above, as a case study. We make use of mass-resolved REMPI data for two-photon resonance excitation to both states,[21] as well as velocity map images of H^+ for resonance excitation to the Rydberg state, as a function of J'. Energy-level-dependent state mixing of the resonance excited states is quantified and photoexcitation processes, leading to H^+ formation, are characterized in terms of states and fragmentation processes involved, depending on the state mixing.

This journal is © the Owner Societies 2016

II. Experimental

VMI

The VMI setup used in this work has been described previously.[40,41] A molecular beam of HBr is formed by a 15–30% HBr mixture in He expanding through a homemade piezo-electrically actuated nozzle valve (1 mm diameter) and is skimmed before entering the detection chamber where the ion optics are positioned. Appropriate conditions (*e.g.* denser mixtures and/or use of the hotter part of the molecular beam) were used to probe high J states. After passing through a 2 mm diameter hole in the repeller electrode, the molecular beam is intersected at right angles by a laser beam focused at the geometric focus position of a single-electrode repeller-grid arrangement. The laser beam is generated by an Nd^{3+}:YAG pumping a master oscillator power oscillator system (Spectra Physics MOPO, 0.2 cm^{-1} linewidth, FWHM). The energy per pulse was ~2 mJ and the pulse duration was typically 10 ns (FWHM). The laser beam (~5 mm in diameter) was focused using a 30 cm lens on the molecular beam. Laser polarization is parallel to the detector plane and perpendicular to the molecular beam propagation direction.

For the VMI experiments reported here, the repeller is always ON, *i.e.*, the apparatus is operated in the "VMI mode". The photofragments traverse a field-free time-of-flight region (45 cm) and a gated, position-sensitive detector (dual, imaging-quality MCP array coupled to a phosphor screen) images the photofragment sphere. The image frame is recorded asynchronously every second (~10 laser shots) using a CCD camera and several thousand frames are averaged to form velocity map images. The 2D slice of the 3D ion distribution from each final image is extracted by inverse Abel transformation and integrated from its center over angle to extract the speed, and over radius to extract the angular distributions of the photofragments.

H^+ photoion images are recorded following HBr two-photon excitation in steps of 0.005 nm for a laser excitation in the wavelength region of 235.816–235.926 nm. Background images are recorded with the laser on and the molecular beam off and subtracted from the signal images.

III. Results

A. Mass resolved REMPI

Rotational peaks due to resonance transitions to the 6pπ $^3\Sigma^-(0^+;\ v' = 0)$ (O, Q and S lines) and $V^1\Sigma^+(0^+,\ v' = m + 17)$ states of $H^{79}Br$ and $H^{81}Br$, as well as some bromine atomic lines, appear in the two-photon excitation region of 84 740–85 120 cm^{-1}.[21,42] The observed Q lines of the 6pπ(0) spectrum are found to appear between those for $J' = 7$ and 8 of the V(m + 17) spectrum. While the rotational lines of the $H^{79}Br$ and $H^{81}Br$ molecules, for the same J' quantum numbers, overlap for the 6pπ(0) Rydberg state spectrum, those of the V(m + 17) spectrum are separated, due to isotope shift effects. Spectral perturbations, appearing as line-shifts and line-intensity alterations of the $J' = 7$ and 8 lines in the Q line series of the 6pπ(0) spectrum, in particular, are due to interactions between the corresponding near-degenerate energy levels of the 6pπ(0) and V(m + 17) states.

Line shift effects. Rotational energy levels ($E_{J'}(1)$ and $E_{J'}(2)$), of the two states, 6pπ(0) (labelled 1) and V(m + 17) (labelled 2), have been derived from the spectra.[21,42] A simplified two-state deperturbation analysis of the spectra, based on the diagonalization of the Hamiltonian matrix elements for the state interactions, described in more detail in ref.23, 29 and 31, revealed a moderate interaction strength of about W_{12} = 7.0 cm^{-1} and the zero order energies ($E^0_{J'}(i)$; i = 1, 2) corresponding to the non-perturbed states. Furthermore, the analysis allowed the determination of improved (zeroth order) spectroscopic constants for the 6pπ(0) state, ν^0 = 84 810 cm^{-1}, B' = 7.89 ± 0.03 cm^{-1} and D' = +0.0004 cm^{-1}. Fig. 2a shows the energy difference between the perturbed and the non-perturbed energy levels ($E_{J'}(i) - E^0_{J'}(i)$) as a function of J' for both states, *i.e.*, a "reduced term value plot". The graph of the 6pπ(0) state shows a typical effect of a near-degenerate interaction with an ion-pair state, which appears as a gradually increasing negative difference in $E_{J'}(1) - E^0_{J'}(1)$ from J' = 4 to 7 followed by an upward jump for J' = 8 and a decrease for J' = 9. This is due to an interaction between

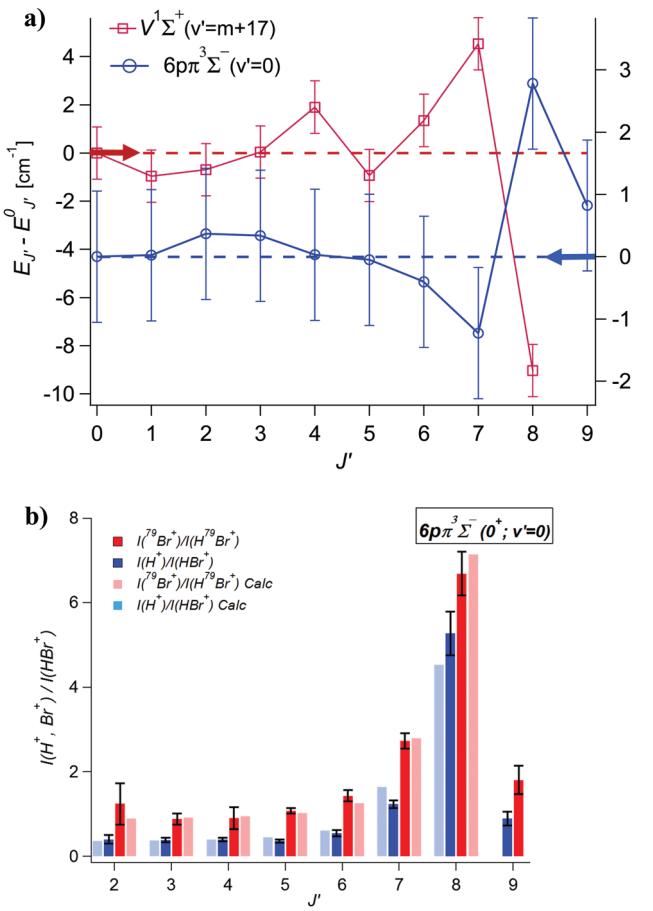

Fig. 2 (a) Line shift (LS) effects: reduced term value plots for the 6pπ(0) and V(m + 17) states derived from perturbed ($E_{J'}$) and deperturbed ($E^0_{J'}$) energy levels for $H^{81}Br$. (b) Line intensity (LI) effects: experimental and calculated relative ion-signal intensities $I(H^+)/I(HBr^+)$ (blue) and $I(^{79}Br^+)/I(H^{79}Br^+)$ (red)) derived for the Q rotational lines for the 6pπ(0) state. An interaction strength of W_{12} = 7.0 cm^{-1} between the 6pπ(0) and V(m + 17) states was assumed in the calculations.

levels of the same J' quantum numbers which results in level repulsions which increase as the energy difference ($|\Delta E_{J'}| = |E_{J'}(1) - E_{J'}(2)|$) between the levels decreases. Based on the number of observations for the ion-pair states of hydrogen halides[21,23,24,29,30] the V(m + 17) state is likely to interact with a number of Rydberg states which could explain a larger irregularity in the ''reduced term value plot'' for the V(m + 17) state. Nevertheless, a ''near mirror effect'' is seen in the plots for J' = 6–8, such that increases in values for V(m + 17) correspond to decreases in the corresponding values for the 6pπ(0) state and *vice versa*. This is a clear indication that the observed near-degenerate interaction found for the 6pπ(0) state is indeed due to mixing with the V(m + 17) state.

Line intensity effect. Fig. 2b shows the ion intensity ratios $I(Br^+)/I(HBr^+)$ and $I(H^+)/I(HBr^+)$ as a function of J' for the Q lines of the 6pπ(0) spectrum. Since fragment ion formations are favoured in long-range/ion-pair state excitations (see Introduction) the sharp increase in the ratios, observed for $J' \sim 8$, is also an indication of a near-degenerate interaction between the 6pπ(0) and V(m + 17) states. Furthermore, the graphs could be reproduced reasonably well by a corresponding model function, which depends on the interaction strength (W_{12} = 7.0 cm^{-1}) and the energy differences, $\Delta E_{J'}$,[19,20,26,29,31,43] as shown in Fig. 2b.

Finally, the fractional mixing of the states, ${c_1}^2$ and ${c_2}^2$, which depends on W_{12} and $\Delta E_{J'}$,[17,19,20,22,29,43,44] was evaluated. As seen in Table 1 the percentage mixing of the ion-pair state with the Rydberg state reaches a small, but significant, maxima of about 4.7% and 1.7% for the J' = 8 and 7 levels, respectively.

B. Velocity map imaging (VMI)

H^+ images and kinetic energy release (KER) spectra. H^+ images were recorded for two-photon resonance excitation from the ground state, $X^1\Sigma^+(0^+;\ v' = 0)$, to the 6pπ $^3\Sigma^-(0^+;\ v' = 0)$ Rydberg state in steps of 0.005 nm for a laser excitation in the wavelength region of 235.816–235.926 nm, which covers the two-photon excitations ($2h\nu$) for $J' = J'' = 0$–8 (Q lines) ($2h\nu$ = 84772.3–84811.9 cm^{-1}). The H^+ signals for two-photon resonance excitations to the $V^1\Sigma^+(v' = m + 17)$ ion-pair state, on the other hand, were too weak to allow H^+ images to be recorded. All the images show rings which could be identified as being due to the four major channels for H^+ formation, H*(n = 2) + Br* (1a), H*(n = 2) + Br (1b), HBr^{+}*(v^+) (2a) and $HBr^+(v^+)$ (2b) (see the text in Introduction and Fig. 1), where the ring intensities, hence the kinetic energy release (KER's), change as 1(a) < 1(b) < 2(a) ≈ 2(b). Furthermore, for the longest excitation wavelength region (λ = 235.896–235.926 nm; $2h\nu$ = 84772.3–84783.1 cm^{-1}) a ring of low KER was observed, which is assigned to the path

$$HBr^{\#} \rightarrow H^{**}(n = 3) + Br;\ \text{dissociation},$$

$$H^{**}(n = 3) + h\nu \rightarrow H^+ + e^-;\ \text{photoionization channel } H^{**} + Br. \quad (4)$$

Selected images (for λ = 235.841, 235.886 and 235.911 nm), along with the corresponding KER spectra, are shown in Fig. 3. Fig. 4a shows all the KER spectra stacked according to the varying two-photon excitation energy along with the H^+ REMPI spectrum (to the right, tilted vertically). KER spectra derived for excitation energies closest to those for the Q rotational lines are highlighted in red in Fig. 4a. The KERs for the channels H** + Br (4), H* + Br* (1a) and H* + Br (1b) are almost independent of the excitation energies, of about 0.014, 1.43 and 1.87 eV, respectively, in agreement with predicted values according to

$$\text{KER}(H^* + Br^*;\ 1a) = 3h\nu + E_{J''} - D_0(HBr) - E(H^*) - E(Br^*) \quad (5a)$$

$$\text{KER}(H^* + Br;\ 1b) = 3h\nu + E_{J''} - D_0(HBr) - E(H^*) \quad (5b)$$

$$\text{KER}(H^{**} + Br;\ 4) = 3h\nu + E_{J''} - D_0(HBr) - E(H^{**}) \quad (5c)$$

where $h\nu$ is the photon energy, $E_{J''}$ is the J''-dependent rotational energy of the ground state, determined from known rotational constants[45] and D_0(HBr) (30 210 cm^{-1} [46]) is the bond energy for HBr. E(H*), E(H**) and E(Br*) are the energies of the H*(n = 2) (82259.158 cm^{-1} [47]), H**(n = 3) (97492.304 cm^{-1} [47]) and Br*(J = 1/2) (3685.24 cm^{-1} [47]) excited state atoms with respect to their ground states. The ''multi-peak structure'' associated with the HBr^{+}* (2a) and HBr^+ (2b) channels, in the range between about 2.0 and 3.6 eV, is due to photodissociation of several vibrational levels of $HBr^+(^2\Pi_{3/2})$ and HBr^{+}*$(^2\Pi_{1/2})$ of increasing quantum numbers v^+ as the KER increases and $v^+(HBr^+) > v^+(HBr^{+}$*). The KERs are calculated according to

$$\text{KER}(HBr^+) = h\nu + \text{IE}(HBr) + \Delta G_0(HBr^+, v^+) - D_0(HBr) - \text{IE}(H) \quad (5d)$$

$$\text{KER}(HBr^{+}*) = h\nu + \text{IE}^*(HBr) + \Delta G_0\,(HBr^{+}*, v^+) - D_0(HBr) - \text{IE}(H) - E(Br^*) \quad (5e)$$

where IE(HBr) (94150.672 cm^{-1} [48]) and IE(H) (109678.77 cm^{-1} [47]) are the ionization energies of HBr and H, respectively, and IE*(HBr) (96796.17 cm^{-1} [48]) is the ionization of HBr with respect to the formation of HBr^{+}*. $\Delta G_0(HBr^+, v^+)$ and $\Delta G_0(HBr^{+}*, v^+)$ are the differences in the vibrational terms for v^+ and $v^+ = 0$ for HBr^+ and HBr^{+}*, respectively.[47] We note that ''double'' or ''split'' rings observed for the Br and Br* channels in some of the images (see, for example, the inner ring corresponding to H* + Br* in Fig. 3), which also result in partial ''splitting'' of the corresponding KER peaks, are due to recoil effects as the hydrogen atoms H* ionize to form $H^+ + e^-$.[49,50]

The relative signal strengths (I_{rel}) of various channels, defined as the integrated signal intensities of the channels (i) ($I(i)$) divided by the total integrated intensities ($\sum I(i)$ (*i.e.* I_{rel}) = $I(i)/\sum I(i)$) differ significantly, depending on the resonance excitation wavenumber (and J') (Fig. 4b). For low J's (($J' < 7$) corresponding to the noninteraction region) the branching

Table 1 $H^{79}Br$: fractional mixing of the Rydberg state 6pπ $^3\Sigma^-(0^+;v' = 0)$ and the ion-pair state $V^1\Sigma^+(0^+, v' = m + 17)$, ${c_1}^2$ and ${c_2}^2$, with respect to the 6pπ $^3\Sigma^-(0^+;v' = 0)$ state as a function of J' for the interaction strength, W_{12} = 7.0 cm^{-1}

J'	2	3	4	5	6	7	8
${c_1}^2$	0.999	0.999	0.999	0.998	0.996	0.983	0.953
${c_2}^2$	0.001	0.001	0.001	0.002	0.004	0.017	0.047

This journal is © the Owner Societies 2016

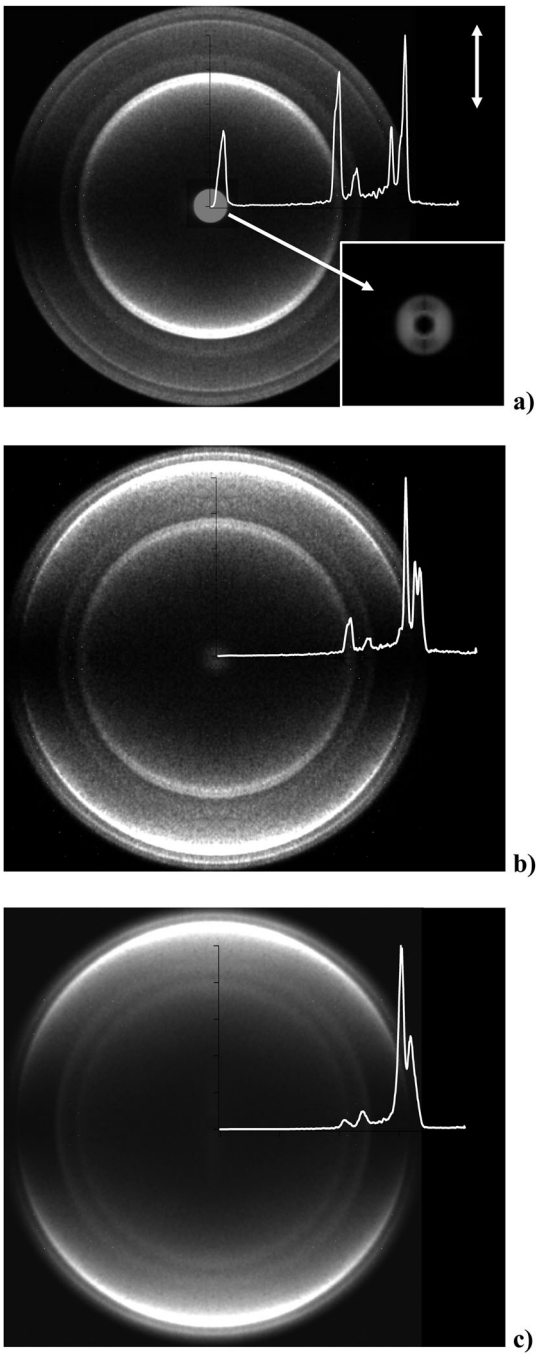

Fig. 3 H^+ velocity map images and kinetic energy release spectra of two-photon resonance excitations *via* the *Q* branch of the 6pπ(0) state spectrum for, (a) 235.911 nm laser excitation/corresponding to excitation to *ca.* the J' = 8 level, (b) 235.886 nm laser excitation/corresponding to *ca.* the J' = 6 level and (c) 235.841 nm laser excitation/corresponding to *ca.* the J' = 2 level. The laser polarization is indicated by the double arrow in (a). The inserted figure in the bottom right corner of (a) shows the 2D (Abel transformed) slice of the innermost ring.

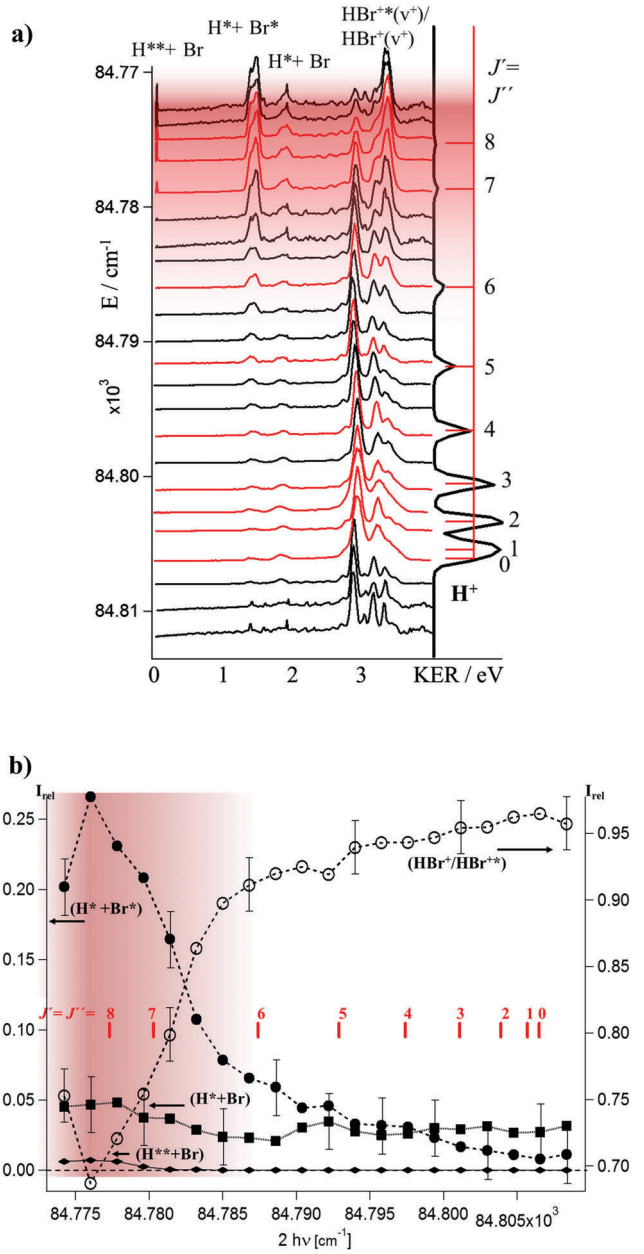

Fig. 4 (a) KERs: stacked kinetic energy release (KER) spectra as a function of two-photon excitation wavenumber along with the H^+ REMPI spectrum of the *Q* lines for the 6pπ(0) state spectrum (tilted to the right). Rotational lines are marked by J'/J'' and KER spectra close to the $J' \leftarrow J''$ resonance transitions are highlighted in red. KER spectra of various H^+ formation channels (H** + Br(4); H* + Br* (1(a)); H* + Br (1(b)); HBr^{+*}/HBr^+ (2(a) and (b)); see the main text) are marked. The area corresponding to the near-degenerate interaction between the 6pπ(0) and V(*m* + 17) states for $J' \approx 7$–8 is shaded in red. (b) Branching ratios: relative integrated H^+ signal intensities (I_{rel}; see the main text) of various H^+ formation channels as a function of the two-photon excitation wavenumber ($2h\nu$). The filled dots refer to the left axis and unfilled dots refer to the right axis, as indicated by arrows. Error bars for selected values are shown. *Q*-rotational line positions of the 6pπ(0) state spectrum are marked by J'/J''. The area corresponding to the near-degenerate interaction between the 6pπ(0) and V(*m* + 17) states for $J' \approx 7$–8 is shaded in red.

fractions of the H* + Br/Br* and H** + Br channels are small or negligible (0–0.04) and the HBr^{+*}/HBr^+ channels dominate (>0.95). For high J's ($J' \sim 7$–8) corresponding to the interaction region) the branching fractions of the H*/H** + Br channels are only marginally larger (0.01–0.05), whereas those of the H* + Br* and HBr^{+*}/HBr^+ channels have increased (0.20–0.26) and decreased (0.69–0.75) respectively.

Furthermore, the relative signal intensities (I_{rel}) of various channels are found to vary with J' in the following way (see Fig. 4a and b):

(1) I_{rel} for the H* + Br* channel (1a) gradually increases with J' for J' = 0–6, after which it increases rapidly to a maximum value for $J' \sim 8$, followed by a decrease.

(2) I_{rel} for the H* + Br channel (1b) is virtually unchanged with J' for J' = 0–8.

(3) I_{rel} for the HBr^{+}* and HBr^{+} channels (2(a) and 2(b)) shows a near-mirror effect to that for the H* + Br* channel, *i.e.*, it gradually decreases with J' for J' = 0–6, after which it decreases rapidly to a minimum value for $J' \sim 8$, followed by an increase.

(4) A closer look at the HBr^{+}* and HBr^{+} channels reveals that the I_{rel}'s due to lower v^{+}'s (KER < 3 eV) show a sharp decrease with J' for J' =6–8, whereas, the I_{rel}'s due to higher v^{+}'s (KER > 3 eV) show a sharp-increase with J' for J' = 6–8.

(5) I_{rel} for the H** + Br channel (4) only appears just below J' = 7 and reaches a maximum for J' = 8.

Angular distributions of H^{+}. Significant angular distribution variations are observed for the H^{+} ions depending on the rings/channels as well as a function of the resonance excitation energy/J' (Fig. 3). The rings for the HBr^{*+}/HBr^{+} and H* + Br* channels all display shapes corresponding to parallel transitions, whereas the ring for the H* + Br channels are all close to isotropic in shape and the rings for the H** + Br channels exhibit a perpendicular character. A slight trend towards an increasing "perpendicular shape" with J' is observed for the HBr^{*+}/HBr^{+} rings/channels, whereas the opposite effect is found for both the H* + Br* and H* + Br rings/channels.

In an attempt to quantify the anisotropy of the rings/channels the angular distributions were fitted by a simplified expression corresponding to a one-step photodissociation,

$$P(\theta) = A[1 + \beta_2 P_2(\cos(\theta)) + \beta_4 P_4(\cos(\theta))]$$

where P_2 and P_4 are the second and fourth order Legendre polynomials and β_2 and β_4 are the corresponding anisotropy parameters and A is a scaling factor. The beta parameters, being "effective" parameters for the overall photodissociation processes, can then be related to the overall transition symmetry and the corresponding dynamics. The β_2 parameter for various channels as a function of the resonance excitation wavenumber (and J'), seen in Fig. 5, shows variations consistent with the observed trends in the ring shapes mentioned above. They are found to vary largely in value between the limits of −1 and +2, corresponding to purely perpendicular and parallel transitions, respectively. The observed trends are discussed in the next section. The fourth Legendre polynomial coefficient (β_4) was used more in order to improve fits rather than to evaluate vector correlation effects, since multi-photon processes and state interactions are involved. Their values for the H* + Br*/Br (1) and H** + Br (4) channels fluctuate around zero (ranging between −0.4 and +0.4), whereas the values for the HBr^{+}*/HBr^{+} (2) channels are mostly negative (−0.6 to 0). The recoil effect ("peak splitting"), observed due the ejection of the electron during the H* ionization processes in some images, does not significantly affect the beta parameter measured and is within the error bars shown in Fig. 5.

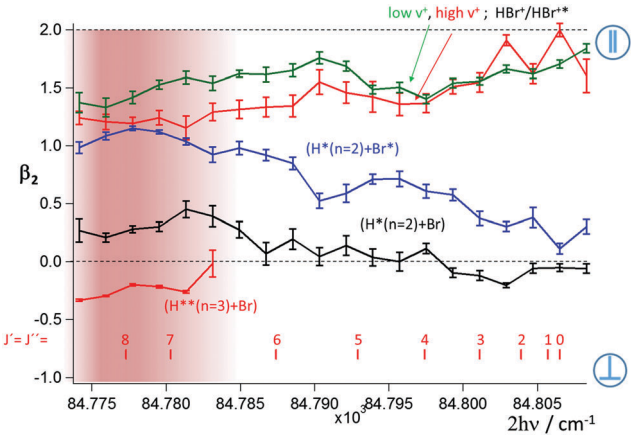

Fig. 5 Angular distributions: anisotropy parameters (β_2) extracted from H^{+} images for various channels (as labelled), by a "single step analysis" of the angular distributions as a function of the two-photon excitation wavenumber. Q-rotational line positions of the 6pπ(0) state spectrum are marked by J'/J''. The limiting values of +2 and −1, for β_2, corresponding to purely parallel (∥) and purely perpendicular (⊥) transitions, respectively, are highlighted. The area corresponding to the near-degenerate interaction between the 6pπ(0) and V(m + 17) states for $J' \approx 7$–8 is shaded in red.

IV. Discussion

The H^{+} formation channels, observed, are all likely to occur *via* one-photon transitions from the 6pπ(0) state ($J' < 7$) or the mixed 6pπ(0)/V(m + 17) state ($J' \sim 7$–8) (HBr^{**}) to repulsive states ($HBr^{\#}$) in the Rydberg series which converges to the ionic states, $B^2\Sigma^+$ and $^2\Pi$[26,30,51] and which correlate with H*(n = 2) + Br*/Br and H**(n = 3) + Br. Considering one-electron transitions and the principal electron configurations ($[\sigma^2\pi^3]6p\pi^1$) and the ($\sigma^1\pi^4\sigma^{*1}$) for the 6pπ(0) and V(m + 17) states, respectively, the Rydberg electron must occupy a 6pπ orbital in which case the possible Rydberg states are $^{1,3}\Pi$ ($[B^2\Sigma^+; \sigma^2(\pi_x^1\pi_y^1)\sigma^{*1}]6p\pi^1$) and $^{1,3}\Sigma$ ($[^2\Pi;\sigma^1\pi^3\sigma^{*1}]6p\pi^1$). The rule of spin conservation will favour the involvement of triplet states in the case of transitions from ($[\sigma^2\pi^3]6p\pi^1$) (corresponding to a pure 6pπ $^3\Sigma^-(0)$ state) and singlet states in the case of transitions from ($\sigma^1\pi^4\sigma^{*1}$) (corresponding to a pure $V^1\Sigma^+$ state). Three major transitions are, therefore, expected to be involved, two from ($[\sigma^2\pi^3]6p\pi^1$) (6pπ $^3\Sigma^-(0)$; dominating short-range excitations) and one from ($\sigma^1\pi^4\sigma^{*1}$) ($V^1\Sigma^+$); longer-range excitations), as (orbital transitions are highlighted, underlined and bold)

(a) $HBr^{**}\{6p\pi^3\Sigma^-([^2\Pi;\sigma^2\underline{\boldsymbol{\pi}}^3]6p\pi^1)\} + h\nu$

$\rightarrow HBr^{\#}\{^3\Pi([B^2\Sigma^+;\sigma^2(\pi_x^1\pi_y^1)\underline{\boldsymbol{\sigma}}^{*1}]6p\pi^1)\}$;

perpendicular core electron transition/$\underline{\boldsymbol{\pi}} \rightarrow \underline{\boldsymbol{\sigma}}^*$

(b) $HBr^{**}\{6p\pi^3\Sigma^-([^2\Pi;\underline{\boldsymbol{\sigma}}^2\pi^3]6p\pi^1)\} + h\nu$

$\rightarrow HBr^{\#}\{^3\Sigma([^2\Pi;\sigma^1\pi^3\underline{\boldsymbol{\sigma}}^{*1}]6p\pi^1)\}$;

parallel core electron transition/$\underline{\boldsymbol{\sigma}} \rightarrow \underline{\boldsymbol{\sigma}}^*$

This journal is © the Owner Societies 2016

(c) $HBr^{**}\{V^1\Sigma(\sigma^1\underline{\pi}^4\sigma^{*1})\} + h\nu$

$\rightarrow HBr^{\#}\left\{{}^1\Sigma\left([^2\Pi;\sigma^1\pi^3\sigma^{*1}]6\underline{p\pi}^1\right)\right\}$; .

parallel core to Rydberg electron transition/$\underline{\pi} \rightarrow \underline{p\pi}$

Based on previous as well as unpublished works relevant to two-photon resonance transitions to $\Omega' = 0$ Rydberg and ion-pair states[26,30,52] there is a reason to believe that the resonance transitions are largely perpendicular (*i.e.* $\Sigma \leftarrow \Pi \leftarrow \Sigma$). Furthermore, there isn't a reason to expect a large variation in the character of those transitions over the relatively short excitation region of concern here (see Fig. 1b). We, therefore, believe that the major variations in the overall parallel *vs.* perpendicular transition characters as a function of J', as well as for the different channels (see above), are associated with the final photodissociation steps following the resonance excitations. Therefore, in the cases of the H* + Br*/Br and H** + Br channels, variations in the transition characters will be determined by the relative contributions of the steps (a)–(c) above. In the case of the $HBr^+/HBr^{+}*$ channels both the steps (a)–(c) and the photodissociation of $HBr^+/HBr^{+}*$ need to be considered.

In light of the above discussion and the results derived from the KER's and the angular distributions, mentioned above, we propose the following major photodissociation processes leading to the formation of various channels.

$HBr^{+}*/HBr^+$

The $HBr^{+}*/HBr^+$ channels dominate for low J'/the non-interaction region (Fig. 4b), suggesting that autoionization processes of the superexcited triplet states $^3\Pi([B^2\Sigma^+]6p\pi^1)$ and $^3\Sigma([^2\Pi_{3/2}]6p\pi^1)$ accessed by the short range transitions from $([\sigma^2\pi^3]6p\pi^1)$ (pure $6p\pi\ ^3\Sigma^-(0)$ state) are more favourable than the alternative dissociation processes to form H* + Br/Br*. Since the overall transitions for the H^+ formation *via* the $HBr^{+}*/HBr^+$ channels are parallel in nature (Fig. 5), the parallel ($\sigma \rightarrow \sigma^*$) transitions (i) from the ground ionic state(s) $HBr^{+}*/HBr^+(X^2\Pi(\sigma^2\pi^3))$ to the $HBr^{+\#}(2^2\Pi(\sigma^1\pi^3\sigma^{*1}))$ state prior to dissociation and ii) for the excitations of the $HBr^{**}(6p\pi^3\Sigma^-([^2\Pi;\sigma^2\pi^3]6p\pi^1))$ to the $HBr^{\#}(^3\Sigma([^2\Pi;\sigma^1\pi^3\sigma^{*1}]6p\pi^1))$ superexcited state are likely to be favoured over the perpendicular ($\pi \rightarrow \sigma^*$) transitions to the $HBr^{+\#}(B^2\Sigma^+;\sigma^2(\pi_x^1\pi_y^1)\sigma^{*1})$ and $HBr^{\#}(^3\Pi([B^2\Sigma^+;\sigma^2(\pi_x^1\pi_y^1)\sigma^{*1}]6p\pi^1))$ states respectively. Therefore, the autoionization process would involve a perpendicular transition of the 6pπ Rydberg electron to the σ valence orbital rather than a parallel transition to a π valence orbital followed by an ejection of an Auger electron from a σ* orbital. The branching fraction of the $HBr^{+}*/HBr^+$ channels as a function of J' closely mirrors that of the H* + Br* channels, by showing a large decrease with increasing J' (*i.e.* by moving from the non-interaction region ($J' < 7$) to the interaction region ($J' \sim 7$–8)). This could be due to joined transitions from the resonance excited state(s) followed by competition between the $HBr^{+}*/HBr^+$ and H* + Br* formation depending on the degree of state mixing. Thus, for low J', dominating triplet-to-triplet short-range transitions from $([\sigma^2\pi^3]6p\pi^1)$ (pure $6p\pi\ ^3\Sigma^-(0)$ state), $HBr^{+}*/HBr^+$ are favoured, whereas for high J's where the weight of long-range transitions from $(\sigma^1\pi^4\sigma^{*1})$ (pure $V^1\Sigma^+$ state; transition) to the $^1\Sigma([^2\Pi_{1/2}]6p\pi^1)$ state increases, and H* + Br* formation is enhanced. The observed sharp decreases in the lower v^+ signals and the corresponding increases in the higher v^+ signals with J' (Fig. 4a) suggest that high v^+ is favoured *via* the long-range transitions from $(\sigma^1\pi^4\sigma^{*1})$ (pure $V^1\Sigma^+$ state; transition). Since the autoionization rate depends on the Franck–Condon-factor overlap between the superexcited repulsive states and the v^+ states of the ionic states, one might, indeed, expect a favourable Franck–Condon-factor overlap between the repulsive states and high v^+ states in the long-range and between repulsive states and low v^+ in the short-range (Fig. 1b).

H* + Br*

A large increase in the branching fraction of the H* + Br* channel (Fig. 4b), and a gradual increase in the parallel character of the corresponding transition (Fig. 5) with increasing J' (*i.e.* by moving from the non-interaction region ($J' < 7$) to the interaction region ($J' \sim 7$–8)), suggests that long-range parallel excitations from $(\sigma^1\pi^4\sigma^{*1})$ (pure $V^1\Sigma^+$ state; transition (c)) to the $^1\Sigma([^2\Pi_{1/2}]6p\pi^1)$ state in the mixing region are of major importance. The very low branching fraction observed for the lowest J' ($J' \sim 0$–2) (Fig. 4b), in fact suggests that the transitions (a) and (b) from $([\sigma^2\pi^3]6p\pi^1)$ (pure $6p\pi\ ^3\Sigma^-(0)$ state) are of minor importance.

H* + Br

The observation of negligible or only small enhancements in the branching fractions of the H* + Br channel (Fig. 4b) and the parallel character of the corresponding transition (Fig. 5) with increasing J' (*i.e.* by moving from the non-interaction region ($J' < 7$) to the interaction region ($J' \sim 7$–8)) suggests that long-range parallel excitations *via* $(\sigma^1\pi^4\sigma^{*1})$ (pure $V^1\Sigma^+$ state; transition (c)) are of minor importance. The values for β_2 of about −0.25 to +0.50 (Fig. 5), however, suggest that both the perpendicular (a) and the parallel transitions (b) from $([\sigma^2\pi^3]6p\pi^1)$ (pure $6p\pi\ ^3\Sigma^-(0)$ state) to the $^3\Pi([B^2\Sigma^+]6p\pi^1)$ and $^3\Sigma([^2\Pi_{3/2}]6p\pi^1)$ states, respectively, are involved.

H** + Br

There is reason to believe that the transitions, prior to the H** + Br formation, are comparable to those of the H* + Br channel, mentioned above for the corresponding superexcited states which correlate with H** + Br (instead of H* + Br). Signals due to the H** + Br channels only appear for high J's ($J' \sim 7$–8). Based on the bond energy of HBr (30 210 ± 40 cm^{-1} [46]) and the energy of H**(n = 3) (97492.3 cm^{-1} [53]) the threshold for the formation of H** + Br from HBr($v'' = 0, J' = 0$) is about 127 702 ± 40 cm^{-1}, which can only be reached *via* $J' > 7$ excitations in Q transitions ($J' = J''$). The three-photon excitations *via* the $J' = 8$ level correspond to the energy of 127 764 cm^{-1}, whereas excitations for lower J's ($J' < 8$) all correspond to energies lower than 127 702 cm^{-1}. In light of this fact, the comparison with the results obtained for the analogous channel of H* + Br above, as well as the overall perpendicular nature of the transition involved (Fig. 5), there is a reason to believe that both the perpendicular (a) and the parallel transitions (b) from

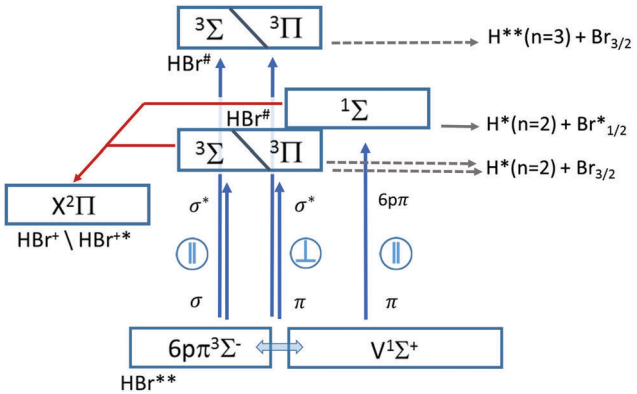

Fig. 6 Schematic figure of the major one-photon transitions (blue arrows) as well as photodissociation (gray arrows) and autoionization (red arrows) processes following two-photon resonance transitions to the 6pπ(0) and 6pπ(0)/V(m + 17) mixed state(s), prior to ionization (see main text). Orbital transitions and the nature (parallel/perpendicular transitions) of the photo-excitations are indicated.

($[\sigma^2\pi^3]6p\pi^1$) (pure 6pπ $^3\Sigma^-(0)$ state) to the $^3\Pi([B^2\Sigma^+]6p\pi^1)$ and $^3\Sigma([^2\Pi_{3/2}]6p\pi^1)$ states, respectively, are involved.

V. Conclusions

A mass resolved and H^+ velocity map imaging analysis of HBr REMPI, in the two-photon resonance excitation region of 84 740–85 120 cm^{-1}, has revealed a clear picture of the effect of triplet to singlet state interactions on photofragmentation processes. Rotational line-shifts and intensity alterations of mass resolved REMPI spectra due to resonance excitations to the 6pπ $^3\Sigma^-(v' = 0)$ Rydberg and $V^1\Sigma^+(v' = m + 17)$ valence (ion-pair) states are indicative of interactions between these states. Deperturbation analysis of the data revealed the interaction strength as well as zero order spectroscopic parameters for the 6pπ $^3\Sigma^-(0)$ state. The fractional mixing is found to vary with J' to reach maxima for the near-resonance levels J' = 7–8. H^+ velocity map images derived as a function of the excitation wavenumber in the region of the Q branch of the 6pπ $^3\Sigma^-(0)$ state spectrum revealed signals due to five major formation channels corresponding to the intermediate species $H^*(n = 2)$ + Br*/Br (1(a) and (b)), $H^{**}(n = 3)$ + Br (4), and $HBr^{+*}(v^+)/HBr^+(v^+)$ (2(a) and (b)) prior to the H* and H** atom photoionization processes (1(a), (b) and 4) and molecular ion (HBr^{+*}/HBr^+) photodissociation processes. Branching fractions and anisotropy parameters were derived from the kinetic energy release (KER) spectra and angular distributions, respectively, as a function of the excitation wavelengths/J'. Considering these data, the KER spectra structural variations as well as the resonance excited state interactions, the following major photoexcitations of the resonance excited state(s) 6pπ $^3\Sigma^-(0)$ mixed with V(m + 17), prior to the H^+ formations, are proposed (see Fig. 6).

For a limited state mixing (pure $[\sigma^2\pi^3]6p\pi\ ^3\Sigma^-(0)$ state/low J') triplet-to-triplet, parallel short-range transitions to a super-excited repulsive $^3\Sigma$ state, followed by autoionization to form $HBr^{+*}(\Omega = 1/2)$ and $HBr^+(\Omega = 3/2)$ dominates over a minor dissociation channel forming H* + Br. A small but significant perpendicular transition to a superexcited repulsive $^3\Pi$ state, followed by dissociation to form H* + Br, is also involved. For an increased state mixing (enhanced $(\sigma^1\pi^4\sigma^{*1})$ $V^1\Sigma^+$ state character/J' = 7–8 in particular) a singlet-to-singlet, parallel long-range transition to a superexcited repulsive $^1\Sigma$ state is brought in followed by autoionization to form $HBr^{+*}(\Omega = 1/2)$ and $HBr^+(\Omega = 3/2)$ as well as dissociation to form H* + Br*. For $J' \sim 8$ triplet-to-triplet, perpendicular and parallel short-range transitions to superexcited repulsive $^3\Pi$ and $^3\Sigma$ states, respectively, followed by dissociation to form H** + Br occur.

Acknowledgements

The financial support from the University Research Fund, University of Iceland and the Icelandic Science Foundation (Grant No. 130259-051) is gratefully acknowledged. The research leading to these results received funding from LASERLAB-EUROPE (grant agreement no. 228334, EC's Seventh Framework Programme). This work was supported by Greek Secretariat for Research and Technology programs ERC03:ITSSUED and THALIS: ISEPUMA, co-financed by EU (European Social Fund) and national funds under NSRF2007–2013. PCS gratefully acknowledges support from an EU Marie Curie Reintegration Grant (GPSDI, Grant No. PIRG07-GA-2010-268305). DZ gratefully acknowledges EU Marie Curie IAPP program SOFORT (GA 251598). We wish to thank Gabriel J. Vázquez, H. P. Liebermann and H. Lefebvre-Brion for useful information concerning HBr potential curves based on unpublished calculations.

References

1 A. E. Douglas and F. R. Greening, *Can. J. Phys.*, 1979, **57**, 1650–1661.
2 D. S. Green, G. A. Bickel and S. C. Wallace, *J. Mol. Spectrosc.*, 1991, **150**, 303–353.
3 D. S. Green, G. A. Bickel and S. C. Wallace, *J. Mol. Spectrosc.*, 1991, **150**, 354–387.
4 D. S. Green, G. A. Bickel and S. C. Wallace, *J. Mol. Spectrosc.*, 1991, **150**, 388–469.
5 D. S. Green and S. C. Wallace, *J. Chem. Phys.*, 1992, **96**, 5857–5877.
6 D. Ascenzi, S. Langford, M. Ashfold and A. Orr-Ewing, *Phys. Chem. Chem. Phys.*, 2001, **3**, 29–43.
7 Á. Kvaran, H. Wang and Á. Logadóttir, *Recent Res. Devel. in Physical Chem.*, Transworld Research Network, 1998, vol. 2, pp. 233–244.
8 Á. Logadóttir, Á. Kvaran and H. Wang, *J. Chem. Phys.*, 1998, **109**, 5856–5867.
9 Á. Logadóttir, Á. Kvaran and H. Wang, *J. Chem. Phys.*, 2000, **112**, 10811–10820.
10 S. G. Tilford and M. L. Ginter, *J. Mol. Spectrosc.*, 1971, **40**, 568–579.
11 M. L. Ginter, S. G. Tilford and A. M. Bass, *J. Mol. Spectrosc.*, 1975, **57**, 271.

 This journal is © the Owner Societies 2016

12 D. S. Ginter, M. L. Ginter and S. G. Tilford, *J. Mol. Spectrosc.*, 1981, **90**, 152.
13 D. S. Ginter, M. L. Ginter, S. G. Tilford and A. M. Bass, *J. Mol. Spectrosc.*, 1982, **92**, 55.
14 D. S. Ginter, M. L. Ginter and S. G. Tilford, *J. Mol. Spectrosc.*, 1982, **92**, 40.
15 J. B. Nee, M. Suto and L. C. Lee, *J. Chem. Phys.*, 1986, **85**, 4919.
16 Á. Kvaran and H. Wang, *J. Mol. Spectrosc.*, 2004, **228**, 143–151.
17 K. Matthiasson, Á. Kvaran, H. Wang, A. Bodi and E. Jónsson, *J. Chem. Phys.*, 2008, **129**, 164313.
18 K. Matthiasson, H. Wang and Á. Kvaran, *J. Mol. Spectrosc.*, 2009, **255**, 1–5.
19 K. Matthiasson, Á. Kvaran and H. Wang, *J. Chem. Phys.*, 2009, **131**, 044324.
20 K. Matthiasson, J. Long, H. Wang and Á. Kvaran, *J. Chem. Phys.*, 2011, **134**, 164302.
21 J. Long, H. Wang and A. Kvaran, *J. Mol. Spectrosc.*, 2012, **282**, 20–26.
22 J. Long, H. R. Hrodmarsson, H. Wang and A. Kvaran, *J. Chem. Phys.*, 2012, **136**, 214315.
23 J. Long, H. Wang and Á. Kvaran, *J. Chem. Phys.*, 2013, **138**, 044308.
24 H. R. Hróðmarsson, H. Wang and Á. Kvaran, *J. Mol. Spectrosc.*, 2013, **290**, 5–12.
25 Y. Xie, P. T. A. Reilly, S. Chilukuri and R. J. Gordon, *J. Chem. Phys.*, 1991, **95**, 854–864.
26 C. Romanescu and H. P. Loock, *J. Chem. Phys.*, 2007, **127**, 124304.
27 S. Kauczok, C. Maul, A. I. Chichinin and K. H. Gericke, *J. Chem. Phys.*, 2010, **133**, 24301.
28 R. Liyanage, R. J. Gordon and R. W. Field, *J. Chem. Phys.*, 1998, **109**, 8374–8387.
29 H. R. Hróðmarsson, H. Wang and Á. Kvaran, *J. Chem. Phys.*, 2014, **140**, 244304.
30 D. Zaouris, A. Kartakoullis, P. Glodic, P. C. Samartzis, H. R. Hróðmarsson and Á. Kvaran, *Phys. Chem. Chem. Phys.*, 2015, **17**, 10468–10477.
31 H. R. Hróðmarsson, H. Wang and Á. Kvaran, *J. Chem. Phys.*, 2015, **142**, 244312.
32 H. Liebel, S. Lauer, F. Vollweiler, R. Muller-Albrecht, A. Ehresmann, H. Schmoranzer, G. Mentzel, K.-H. Schartner and O. Wilhelmi, *Phys. Lett. A*, 2000, **267**, 357–369.
33 P. V. Demekhin, V. L. Sukhorukov, H. Schmoranzer and A. Ehresmann, *J. Chem. Phys.*, 2010, **132**, 204303.
34 Y. Zhou, Q. Meng and Y. Mo, *J. Chem. Phys.*, 2014, **141**, 014301.
35 D. S. Ginter and M. L. Ginter, *J. Mol. Spectrosc.*, 1981, **90**, 177–196.
36 S. T. Pratt and M. L. Ginter, *J. Chem. Phys.*, 1995, **102**, 1882–1888.
37 M. A. Baig, J. Hormes, J. P. Connerade and W. R. S. Garton, *J. Phys. B: At., Mol. Opt. Phys.*, 1981, **14**, L147–L151.
38 R. Callaghan and R. J. Gordon, *J. Chem. Phys.*, 1990, **93**, 4624–4636.
39 C. Romanescu and H.-P. Loock, *Phys. Chem. Chem. Phys.*, 2006, **8**, 2940–2949.
40 C. R. Gebhardt, T. P. Rakitzis, P. C. Samartzis, V. Ladopoulos and T. N. Kitsopoulos, *Rev. Sci. Instrum.*, 2001, **72**, 3848–3853.
41 V. Papadakis and T. N. Kitsopoulos, *Rev. Sci. Instrum.*, 2006, **77**, 5.
42 See ESI†.
43 J. Long, H. Wang and Á. Kvaran, *Acta Phys.-Chim. Sin.*, 2013, **62**, 163302.
44 H. Lefebvre-Brion and R. W. Field, *Perturbations in the Spectra of Diatomic Molecules*, Academic Press, Inc., London, 1986.
45 "Constants of diatomic molecules", NIST Chemistry WebBook, http://webbook.nist.gov/cgi/cbook.cgi?ID=C10035106&Units=SI&Mask=1000, accessed March 2016.
46 P. M. Regan, S. R. Langford, A. J. Orr-Ewing and M. N. R. Ashfold, *J. Chem. Phys.*, 1999, **110**, 281–288.
47 NIST Atomic Spectra Database (ver. 5.3), [Online], http://physics.nist.gov/asd, accessed March 2016, National Institute of Standards and Technology, Gaithersburg, MD.
48 A. J. Yencha, A. J. Cormack, R. J. Donovan, K. P. Lawley, A. Hopkirk and G. C. King, *Chem. Phys.*, 1998, **238**, 133–151.
49 R. L. Toomes, P. C. Samartzis, T. P. Rakitzis and T. N. Kitsopoulos, *Chem. Phys.*, 2004, **301**, 209–212.
50 F. Aguirre and S. T. Pratt, *J. Chem. Phys.*, 2004, **121**, 9855.
51 A. Banichevich, R. Klotz and S. D. Peyerimhoff, *Mol. Phys.*, 1992, **75**, 173–188.
52 D. Zaouris, P. Glodic, P. C. Samartzis, H. R. Hróðmarsson, H. Wang and Á. Kvaran, unpublished work.
53 NIST Chemistry WebBook - NIST Atomic Spectra Database Levels Data, http://webbook.nist.gov/, accessed April 2016.
54 G. J. Vázquez, H. P. Liebermann and H. Lefebvre-Brion, unpublished work.